A New Data Association Method Using Kalman Filter Innovation Vector Projections

Mathieu Joerger
Aerospace and Ocean Engineering
Virginia Tech
Blacksburg, VA, USA
joerger@vt.edu

Ali Hassani
Aerospace and Ocean Engineering
Virginia Tech
Blacksburg, VA, USA
ahassani@vt.edu

***Abstract*—This paper describes the derivation, analysis and implementation of a new data association method that provides a tight bound on the risk of incorrect association for LiDAR feature-based localization. Data association (DA) is the process of assigning currently-sensed features with ones that were previously observed. Most DA methods use a nearest-neighbor criterion based on the normalized innovation squared (NIS). They require complex algorithms to evaluate the risk of incorrect association because sensor state prediction, prior observations, and current measurements are uncertain. In contrast, in this work, we derive a new DA criterion using projections of the extended Kalman filter's innovation vector. The paper shows that innovation projections (IP) are signed quantities that not only capture the impact of an incorrect association in terms of its magnitude, but also of its direction. The IP-based DA criterion also leverages the fact that incorrect associations are known and well-defined fault modes. Thus, as compared to NIS, IPs provide a much tighter bound on the predicted risk of incorrect association. We analyze and evaluate the new IP method using simulated and experimental data for autonomous inertial-aided LiDAR localization in a structured lab environment.**

Keywords—data association, innovation vector, inertial, risk, Kalman filter.

I. INTRODUCTION

GNSS use code division multiple access to unambiguously identify and track multiple signals. But, landmark-based localization requires an additional data association (DA) step to recognize previously observed features, whether these features were just sensed or found in a map [1]. Wrong associations (WA) can lead to large navigation errors [2] that can cause autonomous ground vehicles to collide or crash. In response, in this paper, we derive a new criterion to determine the correct association. Our approach not only mitigates occurrences of WA, but it also provides a tight bound on the risk of incorrection association.

This work is primarily intended for localization of automated driving systems (ADS) using LiDAR and inertial measurement units (IMUs). The focus is on LiDARs for their prevalence in ADS, their market availability, and our prior experience. A raw LiDAR scan is made of thousands of data points, each of which individually does not carry useful navigation information. Raw measurements must be pre-processed before they can be used for navigation [3-6].

A first class of algorithms establishes correlations between successive scans to estimate sensor changes in 'pose' (i.e., position and orientation) [6-9]. One of the most widely implemented approaches is the iterative closest point (ICP) [6]. Such procedures can become inaccurate or cumbersome for ADSs moving over time without loop closure unless a map is available. Occupancy grid maps (OGM) [3,10-12] describe the environment using small cells, each of which either contains an object (i.e., is occupied) or does not. The environment can alternatively be interpreted using probability hypothesis density (PHD), which capture the probability of objects being present at surrounding locations [13]. Combining PHDs with random finite set (RFS) theory can help track objects in cluttered environments [13-16]. In the presence of repetitive patterns such as regularly spaced lamp poles or parked cars on a street, correlation-based algorithms using PHD and/or OGM that aim at minimizing pose estimation errors can converge to local minima [16], which can hinder localization risk evaluation.

A second class of algorithms, which is investigated in this paper, provides sensor localization by tracking recognizable, static features in the perceived environment. Two steps are needed: feature extraction (FE) and DA. FE aims at finding the few most consistently recognizable, viewpoint-invariant landmarks in the raw sensor data. DA aims at assigning landmark features to the corresponding feature parameters stored in a map. Yaakov Bar Shalom's seminal work on DA for multi-target tracking [1] has been successfully implemented, and built upon, in a wide variety of applications including landmark-based navigation [2,17-19], pedestrian detection [20], space situational awareness [21-23], air and land surveillance and collision avoidance [24-26], for example, in traffic management [27]. DA can be challenging in the presence of sensor uncertainty. This is why many advanced DA algorithms were developed in [3,28-30].

Of primary concern in safety-critical autonomous vehicle navigation is the prediction of the risk of WA. Two of the most widely-used methods, the Probabilistic Data Association and the Joint Probabilistic Data Association (JPDA) [31],

978-1-7281-0244-3/20/$31.00 ©2020 IEEE

provide the means to evaluate the probability of correct association. But, these Bayesian approaches evaluate risk given current sample data. They are not well suited for safety-critical applications due to the lack of safety risk prediction capability, and to the problem of bounding the a-posteriori probability of association (a similar issue is encountered in [32]). Another insightful approach is followed in [33]. However, it makes approximations that do not necessarily upper-bound risks, hence, do not guarantee safe operation. Reference [33] also presents exact solutions that could only be evaluated using computationally expensive numerical methods, not adequate for real-time navigation.

To circumvent these issues, in our prior work, we derived an analytical upper bound on the risk of WA, which was used to predict navigation integrity [34]. We tested this method in landmark-based LiDAR localization applications [34,35]. Unfortunately, our ability to predict WA occurrences was limited, i.e., our WA risk bound was loose. Even in a structured lab environment with few, sparsely distributed landmarks, the predicted risk bound was high: we would predict that the situation was unsafe, when the risk was actually low. Only when incorporating extra data from inertial measurement units (IMU) were we able to achieve low risk bounds [36,37].

Our prior work and most methods cited in the above three paragraphs are either directly based on Bar Shalom's DA criterion, which uses the normalized innovation squared (NIS), or on some variant also using a weighted norm of residuals. We describe the innovation vector upfront because it is at the heart of this paper. The innovation vector appears in the extended Kalman filter (EKF), the most widely implemented non-linear sequential estimator.

Let n_T be the number of targets in view. From each target originates a measurement set, for example, the target's position coordinates relative to the sensor. The n_T measurement sets are arranged in a measurement vector $\hat{\mathbf{z}}$. There are ($n_T!$) possible ways that the n_T measurement sets could be arranged in $\hat{\mathbf{z}}$. The innovation vector, and its normalized expression $\boldsymbol{\gamma}_i$ defined below, compares $\hat{\mathbf{z}}$ to a predicted version of $\hat{\mathbf{z}}$, noted $\mathbf{h}(\bar{\mathbf{x}})$. Vector $\mathbf{h}(\bar{\mathbf{x}})$ is a non-linear function of prior target observations and of the sensor state prediction $\bar{\mathbf{x}}$. Vector $\bar{\mathbf{x}}$ is typically made of the sensor's location and orientation in a frame of interest (e.g., in a navigation frame East-North-Up). Simply put, vector $\mathbf{h}(\bar{\mathbf{x}})$ is a prediction of $\hat{\mathbf{z}}$ based on where the sensor is expected to be relative to mapped targets. Subscript i in $\boldsymbol{\gamma}_i$ designates a candidate association: because we do not know the actual ordering of measurements in vector $\hat{\mathbf{z}}$, we must assume that it may be permuted as compared to $\mathbf{h}(\bar{\mathbf{x}})$. Vector $\boldsymbol{\gamma}_i$ can therefore be expressed as:

$$\boldsymbol{\gamma}_i = \mathbf{W}_i\,(\mathbf{A}_i\hat{\mathbf{z}} - \mathbf{h}(\bar{\mathbf{x}})) \quad \text{for} \quad i = 0,\ldots,h \tag{1}$$

where $\mathbf{A}_i$ are permutation matrices, $\mathbf{W}_i \equiv \mathbf{Y}_i^{-1/2}$ with $\mathbf{Y}_i$ being the innovation vector covariance matrix, and $h \equiv n_T! - 1$. We use the notation $i = 0$ for the correct association, which is unknown. Vector $\boldsymbol{\gamma}_i$ is zero mean if and only if $i = 0$ [34]. Thus, a sensible criterion to find the correct association is to take the minimum over all values of i of the norm squared of $\boldsymbol{\gamma}_i$, which is the NIS. The NIS-based method is effective, but has limitations in safety-critical applications.

In this paper, we develop a new approach that departs from traditional NIS methods by using EKF innovation vector projections (IP). This IP approach improves DA performance predictions by providing a significantly tighter bound on the risk of WA as compared to NIS. The IP method relaxes the need for extra sensor data and for complex risk evaluation methods to reduce WA risk prediction.

Throughout the paper, we assume a known model of the measurement and sensor state parameter time-propagation. We limit the scope of the paper to cases where all sensed targets have previously been observed. Procedures for dealing with occluded targets, unwanted objects, and miss-extracted features can be found in [38-40] for the NIS approach. These cases will be addressed for IP-based DA in future work. The current IP approach matches targets as a set, which is sometimes referred to as a 'global nearest neighbor' procedure [23,35,40], as opposed to local nearest neighbor (LNN) that finds sensed targets corresponding to mapped targets one at a time [23,40]. The reason for this choice is that LNN requires setting thresholds, or gates, on local NIS [31,40]. For safety analysis, we are concerned that worst-case associations occurring at the threshold would have to be accounted for, and that their impact on a safety risk bounds (on missed extraction risk) would accumulate over time. The global nearest neighbor approach can be computationally more expensive, but can also be more efficient for safety evaluation than LNN.

Section II of the paper outlines our prior work, and uses a one-dimensional two-target ranging example to illustrate the looseness of the NIS-based WA-risk bound. In Section III, we derive the new DA criterion using IP. IP are signed quantities that not only capture the impact of a WA in terms of its magnitude, as does NIS, but also of its direction. We analyze the NIS versus IP approaches in Sections IV and V using simulated and experimental data, respectively, for autonomous landmark-based inertial-aided LiDAR navigation in a structured environment.

II. Prior Work On Navigation Integrity Risk Evaluation Using Normalized Innovations Squared

This section describes a DA method for autonomous landmark-based vehicle navigation in challenging environments, where GNSS is denied. For the NIS DA criterion, we provide a bound on the probability of correct association (CA), evaluate the looseness of this bound in an example two-landmark scenario, and incorporate it in an analytical integrity risk equation. Throughout the section, we point out limitations of our previously derived NIS-based method. We label these limitations **(L1)** to **(L3)**. They will motivate the development of the new IP method in Section III.

A. Data Association Using NIS

To find the most likely CA, which we label i_*, we select the association candidate that satisfies the nearest-neighbor criterion defined as [1]:

$$i_* \equiv \arg\min_{i=0,\ldots,h} \gamma_i^2 \tag{2}$$

with

$$\gamma_i^2 \equiv \boldsymbol{\gamma}_i^T \boldsymbol{\gamma}_i \tag{3}$$

In [34], we derived an analytical bound on the probability of CA, $P(CA)$. By definition of the DA criterion in (2), a WA occurs if the NIS γ_i^2 for any candidate association $i \neq 0$ is smaller than γ_0^2. We derived the following $P(CA)$-bound in [34]:

$$\begin{aligned} P(CA) &= 1 - P(WA) \\ &= 1 - P\left(\bigcup_{i=1}^{h} \gamma_i^2 \le \gamma_0^2\right) \\ &\ge 1 - P\left(q^2 \ge \frac{y_{MIN}^2}{4}\right) \end{aligned} \tag{4}$$

where

$$y_{MIN}^2 \equiv \min_{i=1,\ldots,h} y_i^2 \quad \text{and} \quad y_i^2 \equiv E\{\gamma_i^2\} \tag{5}$$

In (4), q^2 is a chi squared random variable with $(n+m)$ degrees of freedom, where n is the number of measurements (length of $\hat{\mathbf{z}}$) and m is the number of states (length of $\bar{\mathbf{x}}$). In (5), $E\{\ \}$ designates the expected value operator. The last two sentences point out two limitations of this approach:

(L1) Even though $\boldsymbol{\gamma}_i$ is n-dimensional, we had no choice but to consider a chi squared random variable q^2 with $(n+m)$ degrees of freedom in order to properly account for the correlation of γ_i^2 with γ_0^2 in the second equality in (4) (details can be found in [34]).

(L2) y_i^2 is the mean value of γ_i^2. For $i > 0$, y_i^2 is a measure of separation between targets: the larger y_i^2 is, the better the ability to distinguish targets. y_i^2 is unknown. Our best guess for y_i^2 is the sample γ_i^2. We can use a model of the measurement and state prediction noise to derive a lower bound on y_i^2 that is guaranteed with a risk allocation drawn from the overall integrity risk requirement [34]. This extra step adds complications and contributes to the looseness of the $P(CA)$ bound. To limit the length of the paper, we do not include this step in the paper, but interested readers can find it in [34,39].

The $P(CA)$ bound in (4) is a compact expression. First, the factor '1/4' on the right-hand side was derived from the inverse of the sum squared of the maximum eigenvalues of two idempotent matrices [34]. Second, the bound accounts for all potential WA. To achieve this, we had to take the minimum value of y_i^2 over all possible WA.

(L3) The $P(CA)$ bound does not capture the individual contributions of each WA. Instead, in (5), it takes the minimum of y_i^2 for $i = 1,\ldots,h$. This limitation stems from the fact that (4) considers a union of events involving a chi-squared distributed DA statistic.

B. One-Dimensional Two-Target DA Example Using NIS

To illustrate the looseness of the bound, we use the one-dimensional (1D) example displayed in Fig. 1. The problem is to estimate the scalar position x of the sensor (upward pointing triangle) on a 1D navigation reference axis ***R***, given the positions p_A and p_B of two target landmarks (black circles), and using a set of noisy scalar measurements z_1 and z_2 between sensor and landmarks. The challenge of DA is, in the presence of sensor errors, to find the ordering of landmarks $\{p_A, p_B\}$ corresponding the ordering of measurements $\{z_1, z_2\}$.

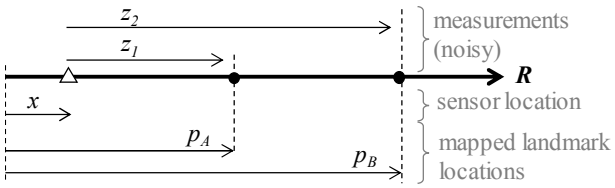

Fig. 1. Illustrative one-dimensional example of a sensor (at location x in reference ***R***) providing observations to two landmarks (at locations p_A and p_B). Sensor to landmark measurements are noted z_1 and z_2.

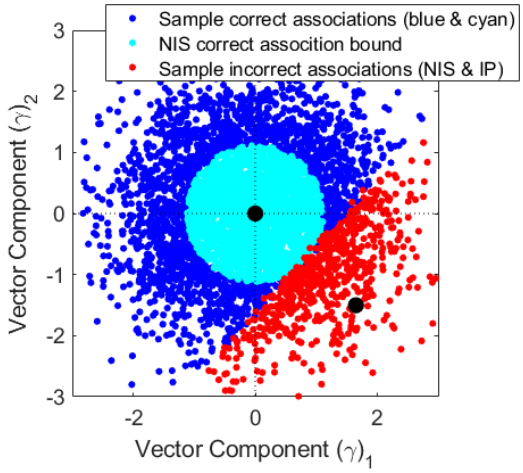

Fig. 2. Two-dimensional normalized innovation-space representation of the association process. The ratio of blue-and-cyan samples over the total number of samples is the actual probability of correct association (CA). Only cyan samples are accounted for in the NIS lower-bound on the probability of CA.

In this instance, the number of target landmarks is $n_T = 2$, and the number of possible permutations is $(n_T!) = 2$, i.e., we consider two innovation vectors $\boldsymbol{\gamma}_0$ and $\boldsymbol{\gamma}_1$. Let us define $\mathbf{y}_0$ and $\mathbf{y}_1$ as the mean vectors of $\boldsymbol{\gamma}_0$ and $\boldsymbol{\gamma}_1$. Because index 0 designates the CA, $\mathbf{y}_0 = \mathbf{0}$, but $\mathbf{y}_1 \neq \mathbf{0}$.

The DA criterion in (2) is represented in Fig. 2 in normalized innovation space, which is two-dimensional ($n = 2$). Vectors $\mathbf{y}_0$ and $\mathbf{y}_1$ are represented with black dots, and $\mathbf{y}_0$ is at the origin. In addition, 5000 random samples of innovation vectors are displayed. The innovation vectors are normalized, which explains the isotropic sample distribution. The criterion in (2) was directly used to distinguish correctly associated samples in blue-and-cyan, from incorrectly associated samples in red. The actual $P(CA)$ is the ratio of blue-and-cyan samples over the total number of samples. In addition, cyan dots represent correctly associated samples as counted using the bound in (4). We simulated measurement and state prediction noise with a large variance as compared to the target separation. In this particular example, the $P(CA)$ lower-bound bound only counted 26% of samples when in actuality, 87% were correctly associated. This direct simulation illustrates observation **(L3)**.

C. Example Application: Integrity Risk Bound Using NIS

In prior work, we used the $P(CA)$ -bound to quantify landmark-based navigation integrity in automotive applications [34]. The integrity risk, or probability of hazardously misleading information (HMI) at time k, is noted $P(HMI_k)$, and is defined in Fig. 3. The safety criterion is: $P(HMI_k) \leq I_{REQ,k}$ where $I_{REQ,k}$ is a predefined integrity risk requirement set by a certification authority (similar to requirements set for aviation applications in [41-43]). Values for $I_{REQ,k}$ that might be used in future autonomous driving system (ADS) applications can be found in [44-46].

In [34,39], we established an analytical bound on the integrity risk, which accounts for the risk of any incorrect association at any time. This bound is expressed as:

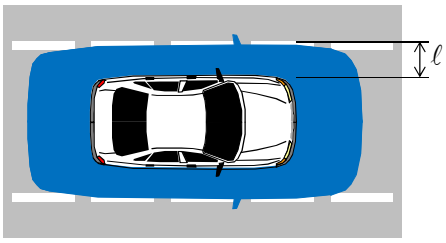

Fig. 3. Integrity Risk for Automotive Applications. The integrity risk is the probability of the car being outside the alert limit requirement box (blue shaded area) when it was estimated to be inside the box. When lateral deviation is of primary concern, then the alert limit is the distance ℓ between edge of car and edge of lane.

$$P(HMI_k) \leq 1 - \left[1 - P(HMI_k \mid CA_K)\right] P(CA_K) \tag{6}$$

with

$$P(HMI_k \mid CA_K) = 2Q\left\{\ell / \sigma_k\right\} \tag{7}$$

$$P(CA_K) \geq \prod_{l=1}^{k} P_{\chi^2}\left\{n_l + m_l \ , \ \frac{y_{MIN}^2}{4}\right\} \tag{8}$$

where

- k is an index identifying a time step;
- K designates a range of indices: $K \equiv \{0,...,k\}$, from filter initiation to time k;
- CA_K is the correct association hypothesis for all landmarks, at all times 0, ..., k;
- $Q\{\ \}$ is the tail probability function of the standard normal distribution;
- ℓ is the specified alert limit that defines a hazardous situation [44-46] (e.g., see Fig. 3);
- σ_k is the standard deviation of the estimation error for the vehicle state of interest (or linear combination of states);
- $P_{\chi^2}\{dof, T\}$ is the probability that a chi-squared-distributed random variable with "*dof*" degrees of freedom is lower than some value T;
- n_l is the number of measurements at time step l;
- m_l is the number of estimated state parameters at time l;

In an EKF, because past-time WA can impact current-time state estimates, we must account for WA at all time steps from EKF initialization to current-time. This raises an additional concern.

Limitations **(L1)** to **(L3)** are the motivation for seeking a new approach, one that is not based on chi-square distributed random variables.

III. A New Approach Using Innovation Vector Projections

In order to address the limitations of the NIS-based method, we develop a new method that uses innovation projections (IP).

A. New Data Association Criterion Using IP

To avoid dealing with chi-squared variables, we project vectors $\boldsymbol{\gamma}_i$ to obtain a DA test statistic that is a linear combination of normally distributed random variables. Given that projections are signed quantities and that WA are well-structured sources of error, we will be able to leverage the direction of these errors to help identify them.

The first question is: what vector should $\boldsymbol{\gamma}_i$ be projected on? In innovation space, e.g., in Fig. 2, the obvious direction is

along $\mathbf{y}_1$. Vector $\mathbf{y}_1$ is unknown, but our best a-priori guess on $\mathbf{y}_1$, or $\mathbf{y}_j$ in general, is given by:

$$\overline{\boldsymbol{\gamma}}_j = \mathbf{W}_j(\mathbf{A}_j - \mathbf{I})\mathbf{h}(\overline{\mathbf{x}}) \quad \text{for} \quad j = 1,...,h \tag{9}$$

where $\mathbf{I}$ is the $n \times n$ identity matrix and where we introduced the index j. We consider projections along all characteristic WA directions $\mathbf{y}_j$, or along our best guess, $\overline{\boldsymbol{\gamma}}_j$. The idea is to increase our chances of identifying WA by projecting $\boldsymbol{\gamma}_i$ along a direction that maximizes the projection's magnitude, i.e., ideally along $\mathbf{y}_i$. In contrast, for the CA, projections of the zero-mean $\boldsymbol{\gamma}_0$ along any direction should be small. It is worth noticing that index j, for $j = 1,...,h$, is known because we can generate the permutation matrices $\mathbf{A}_j$. But, which of index i is $i = 0$ remains unknown because the sample innovation vector is affected by measurement and state prediction error. (We can generate a comprehensive set of permutations to $\boldsymbol{\gamma}_i$'s, for $i = 0,...,h$, but we do not know which of these is the CA).

The second question is: how to choose a criterion that combines all projections along $\overline{\boldsymbol{\gamma}}_j$, for $j = 1,...,h$. After first considering the maximum projection, we settled on the sum of projections because it would help us evaluate a $P(CA)$ -bound.

Therefore, the IP-based DA approach identifies the CA i_* using the following criterion:

$$i_* \equiv \arg\min_{i=0,...,h} \left(\boldsymbol{\beta}^T \boldsymbol{\gamma}_i\right) \quad \text{where} \quad \boldsymbol{\beta} \equiv \sum_{j=1}^{h} \overline{\boldsymbol{\gamma}}_j \tag{10}$$

This expression involves more terms than the NIS criterion in (2): we compute vectors $\boldsymbol{\gamma}_i$, for $i = 0,...,h$ as well as $\overline{\boldsymbol{\gamma}}_j$, for $j = 1,...,h$. But the effectiveness of the resulting approach is worth the computational cost if $P(CA)$ -evaluation is of interest. The next subsection provides an analytical lower bound on $P(CA)$ using IP.

B. Analytical Bound on the Probability of CA Using IP

The starting point of the derivation is the following. A WA-event using the IP criterion in (10) occurs when the following inequality is always satisfied:

$$\boldsymbol{\beta}^T \boldsymbol{\gamma}_i \le \boldsymbol{\beta}^T \boldsymbol{\gamma}_0 \quad \text{for any } i,\ i = 1,...,h \tag{11}$$

In order to evaluate the probability of occurrence of the WA event, we respectively define the actual measurement and predicted measurement vectors as:

$$\hat{\mathbf{z}} = \mathbf{z} + \mathbf{v} \quad \text{and} \quad \mathbf{h}(\overline{\mathbf{x}}) = \mathbf{h}(\mathbf{x}) + \mathbf{H}\boldsymbol{\varepsilon} \tag{12}$$

where $\mathbf{z} \equiv \mathrm{E}\{\hat{\mathbf{z}}\}$, $\mathbf{h}(\mathbf{x}) \equiv \mathrm{E}\{\mathbf{h}(\overline{\mathbf{x}})\}$, $\mathbf{H} \equiv \left.\dfrac{\partial \mathbf{h}(\mathbf{x})}{\partial \mathbf{x}}\right|_{\overline{\mathbf{x}}}$ (13)

with $\mathrm{E}\{\ \}$ being the expectation operator. The measurement noise vector $\mathbf{v}$ is assumed normally distributed with zero mean and covariance $\mathbf{V}$. We use the notation: $\mathbf{v} \sim \mathrm{N}(\mathbf{0},\ \mathbf{V})$. We assume that the state prediction error vector $\boldsymbol{\varepsilon} \equiv \overline{\mathbf{x}} - \mathrm{E}\{\overline{\mathbf{x}}\}$ satisfies: $\boldsymbol{\varepsilon} \sim \mathrm{N}(\mathbf{0},\ \overline{\mathbf{P}})$. We can use these notations to express the innovation covariance matrix as: $\mathbf{Y}_i \equiv \mathbf{A}_i \mathbf{V} \mathbf{A}_i^T + \mathbf{H}\overline{\mathbf{P}}\mathbf{H}^T$.

The following inequalities are equivalent to (11):

$$\boldsymbol{\beta}^T[\boldsymbol{\gamma}_i - \boldsymbol{\gamma}_0] \le \mathbf{0}$$

$$\boldsymbol{\beta}^T\left[\mathbf{W}_i(\mathbf{A}_i\hat{\mathbf{z}} - \mathbf{h}(\overline{\mathbf{x}})) - \mathbf{W}_0(\mathbf{A}_0\mathbf{v} - \mathbf{H}\boldsymbol{\varepsilon})\right] \le \mathbf{0}$$

$$\boldsymbol{\beta}^T\left[\mathbf{W}_i(\mathbf{A}_i\mathbf{z} + \mathbf{A}_i\mathbf{v} - \mathbf{h}(\mathbf{x}) - \mathbf{H}\boldsymbol{\varepsilon}) - \mathbf{W}_0(\mathbf{A}_0\mathbf{v} - \mathbf{H}\boldsymbol{\varepsilon})\right] \le \mathbf{0} \tag{14}$$

By definition of a CA (subscript $i = 0$), $\mathrm{E}\{\boldsymbol{\gamma}_0\} = \mathbf{0}$, which is equivalent to:

$$\mathbf{A}_0\mathbf{z} = \mathbf{h}(\mathbf{x}), \quad \text{or} \quad \mathbf{z} = \mathbf{A}_0^T\mathbf{h}(\mathbf{x}) \tag{15}$$

Substituting (15) into (14) gives the following inequality:

$$\boldsymbol{\beta}^T\left[\mathbf{W}_i(\mathbf{A}_i\mathbf{A}_0^T\mathbf{h}(\mathbf{x}) - \mathbf{h}(\mathbf{x}) + \mathbf{A}_i\mathbf{v} - \mathbf{H}\boldsymbol{\varepsilon}) - \mathbf{W}_0(\mathbf{A}_0\mathbf{v} - \mathbf{H}\boldsymbol{\varepsilon})\right] \le \mathbf{0} \tag{16}$$

After re-arranging terms, (16) becomes:

$$\zeta_i \le T_i \tag{17}$$

where $\zeta_i \equiv \boldsymbol{\beta}^T\left[(\mathbf{W}_i\mathbf{A}_i - \mathbf{W}_0\mathbf{A}_0)\mathbf{v} - (\mathbf{W}_i - \mathbf{W}_0)\mathbf{H}\boldsymbol{\varepsilon}\right]$

$$T_i \equiv -\boldsymbol{\beta}^T\mathbf{W}_i(\mathbf{A}_i\mathbf{A}_0^T - \mathbf{I})\mathbf{h}(\mathbf{x})$$

The distribution of ζ_i is known:

$$\zeta_i \sim \mathrm{N}(0\ , \sigma_i^2) \tag{18}$$

where

$$\sigma_i^2 \equiv \boldsymbol{\beta}^T(\mathbf{W}_i\mathbf{A}_i - \mathbf{W}_0\mathbf{A}_0)\mathbf{V}(\mathbf{W}_i\mathbf{A}_i - \mathbf{W}_0\mathbf{A}_0)^T\boldsymbol{\beta} + \boldsymbol{\beta}^T(\mathbf{W}_i - \mathbf{W}_0)\mathbf{H}\overline{\mathbf{P}}\mathbf{H}^T(\mathbf{W}_i - \mathbf{W}_0)^T\boldsymbol{\beta}$$

Equation (17) can be used to evaluate the probability of the WA event occurring for a given *i,* for example for comparison with the expressions in (4) and (5).

In practice, $\mathbf{h}(\mathbf{x})$ is unknown; our best guess of $\mathbf{h}(\mathbf{x})$ is $\mathbf{h}(\overline{\mathbf{x}})$. A similar problem appeared for NIS, which was pointed out in **(L2)**. Fortunately, the IP method offers a straightforward and efficient way to address the loose bound described in **(L2)**. Substituting the equation $\mathbf{h}(\mathbf{x}) = \mathbf{h}(\overline{\mathbf{x}}) - \mathbf{H}\boldsymbol{\varepsilon}$

in T_i , substituting the result into (17), and rearranging terms, we obtain the following inequality:

$$\zeta_{N,i} \le T_{N,i} \tag{19}$$

where $\zeta_{N,i} \equiv \boldsymbol{\beta}^T \left[(\mathbf{W}_i \mathbf{A}_i - \mathbf{W}_0 \mathbf{A}_0)\mathbf{v} - (\mathbf{W}_i \mathbf{A}_i \mathbf{A}_0^T - \mathbf{W}_0)\mathbf{H}\boldsymbol{\varepsilon} \right]$

$$T_{N,i} \equiv -\boldsymbol{\beta}^T \mathbf{W}_i (\mathbf{A}_i \mathbf{A}_0^T - \mathbf{I})\mathbf{h}(\bar{\mathbf{x}})$$

The distribution of $\zeta_{N,i}$ is $\zeta_{N,i} \sim \mathrm{N}(0, \sigma_{N,i}^2)$, where:

$$\sigma_{N,i}^2 \equiv \boldsymbol{\beta}^T (\mathbf{W}_i \mathbf{A}_i - \mathbf{W}_0 \mathbf{A}_0)\mathbf{V}(\mathbf{W}_i \mathbf{A}_i - \mathbf{W}_0 \mathbf{A}_0)^T \boldsymbol{\beta} + \boldsymbol{\beta}^T (\mathbf{W}_i \mathbf{A}_i \mathbf{A}_0^T - \mathbf{W}_0)\mathbf{H}\bar{\mathbf{P}}\mathbf{H}^T (\mathbf{W}_i \mathbf{A}_i \mathbf{A}_0^T - \mathbf{W}_0)^T \boldsymbol{\beta}$$

For clarity of explanation and to limit the length of the paper, we use equations (1) to (5) for NIS and the inequality in (17) rather than (19) for the IP approach. We are able to do so in the "Testing and Experimental Evaluation" because reference truth is available. Even though this extra benefit of the IP method's ability to address **(L2)** is not be leveraged, it will still outperform NIS.

By definition of a WA in (11), we can write the following expression:

$$\begin{aligned} P(CA) &= 1 - P(WA) \\ &= 1 - P\left(\bigcup_{i=1}^{h} \boldsymbol{\beta}^T \boldsymbol{\gamma}_i \le \boldsymbol{\beta}^T \boldsymbol{\gamma}_0 \right) \\ &\ge 1 - \sum_{i=1}^{h} \left(\zeta_i \ge T_i \right) \\ &\ge 1 - \sum_{i=1}^{h} Q\left\{ T_i / \sigma_i \right\} \end{aligned} \tag{20}$$

In (20), the probability of a union of events is upper-bounded by the sum of probabilities of each individual event. This will cause a loose bound in cluttered environment when measurements and state predictions are highly uncertain, i.e., when the actual WA risk is high. The bound will be tight when it matters, i.e., when the actual risk is low enough to approach or meet safety-critical requirements.

C. One-Dimensional Two-Target DA Example Using IP

We evaluated the IP method by direct simulation for the 1D example in Fig. 1. For each association hypothesis, the IP criterion in (10) separates the innovation hyperspace, which is a plane in Fig. 2, in a half space for CA and the other half space for WA. In contrast, the NIS criterion in (2) identifies CA within a hypersphere (a circle in Fig. 2) of radius the half-magnitude of the smallest mean innovation vector. The IP criterion produced the same WA red samples in Fig. 2 as NIS, which means that the *actual* WA risk is the same using both methods. However, the IP CA *bound* in (20) gave 86.9%, which accurately estimated the *actual* sample CA probability of 87% (ratio of blue-&-cyan samples over all samples), much more so than the 26% NIS bound obtained using (4).

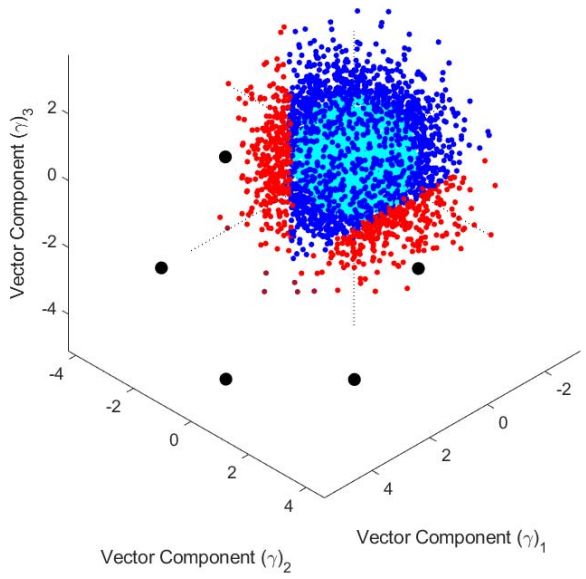

Fig. 4. Three-dimensional normalized innovation-space representation of the association process. The ratio of blue-and-cyan samples over the total number of samples is the actual probability of correct association (CA). Only cyan samples are accounted for in the NIS lower-bound on the probability of CA, whereas both blue and cyan samples are accounted for using IP. Few maroon data points (bottom left of the sample ball) are double counted using the IP bound.

The 1D example in Fig. 1 was extended to include a third landmark. The separation between pairs of adjacent landmarks was taken to be the same. Values of the actual distance between landmarks, measurement error and state prediction variance, are inconsequential in this preliminary discussion. Thus, in Fig. 4, the innovation space is three-dimensional (n_T = 3) and the number of innovation permutations is n_T ! = 6. The 6 mean innovation vectors are represented with black dots. Red samples represent incorrectly associated cases, which again match for the NIS and IP approaches. Cyan dots representing the NIS CA bound are not easy to distinguish, but they are within a sphere centered at the origin. In contrast, the IP CA bound is more accurate because it can be represented as including both cyan and blue samples. Six maroon data points at the bottom left of the sample-ball are double or triple counted using the IP bound because they lay in overlapping half-spaces as defined in (17) for $i = 1,...,h$. In this example, the actual CA probability was 88.2%, well approximated by the IP bound with 88%, whereas the NIS bound gave 35.5%.

IV. Risk Bound Analysis Using Simulated Data

This section compares NIS versus IP DA criteria in an example application of landmark-based LiDAR/IMU navigation, for a vehicle roving between landmarks. We assume that the initial rover position is known, and that a map is available. The EKF-based algorithm is detailed in [37]. We use this simulation to illustrate how the IP method addresses the NIS limitations. A two-landmark scenario illustrates the difference in NIS versus IP DA risk bounds and assesses the looseness of the NIS bound as pointed out in **(L1)** to **(L3)**.

In Fig. 5, a rover whose location over time is shown with black triangles drives by two point-feature landmarks represented with black circles. The vehicle is equipped with a LiDAR/IMU system with specifications given in Table I. We picked error model parameter values, in particular a large LiDAR range error standard deviation, in order to facilitate risk evaluation by direct simulations using a tractable number of random samples. The red ellipses in Fig. 5 are inflated by a factor 75 to facilitate visualization. They represent the rover's positioning errors. The ellipses' shape and dimensions vary as the LiDAR-to-landmark geometry changes due to rover motion. The impact of geometry changes on lateral positioning deviations, which are of primary concern in this paper, are analyzed in detail in [2].

TABLE I. LIDAR AND IMU SIMULATION PARAMETERS

System Parameters	Values
Standard deviation of LiDAR feature range data	0.3 m
Standard deviation of LiDAR feature angular data	0.5 deg
LiDAR data sampling interval	0.5 s
Accelerometer velocity random walk	0.022 m/s^2/$\sqrt{\text{Hz}}$
Gyroscope angle random walk	0.15 deg/$\sqrt{\text{hr}}$
Accelerometer time constant	3600 s
Gyroscope time constant	3600 s
Standard deviation of accelerometer GMRP bias	0.1 m/s^2
Standard deviation of Gyroscope GMRP bias	0.2 deg
Vehicle speed	1 m/s
Alert limit ℓ	0.25 m

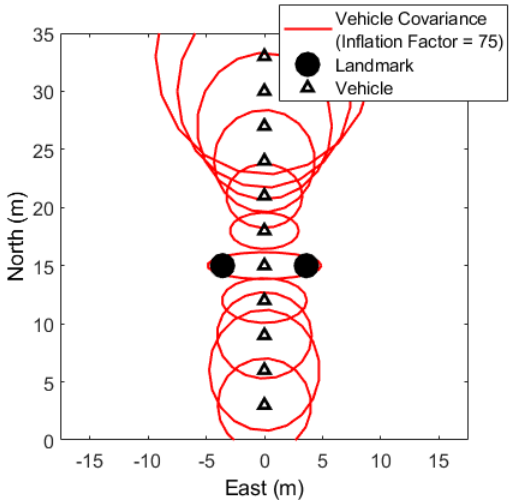

Fig. 5. Vehicle and Landmark Positioning Covariance Analysis Using LiDAR/IMU in EKF-Based Simultaneous Localization And Mapping (SLAM) for the Two-Landmark Scenario.

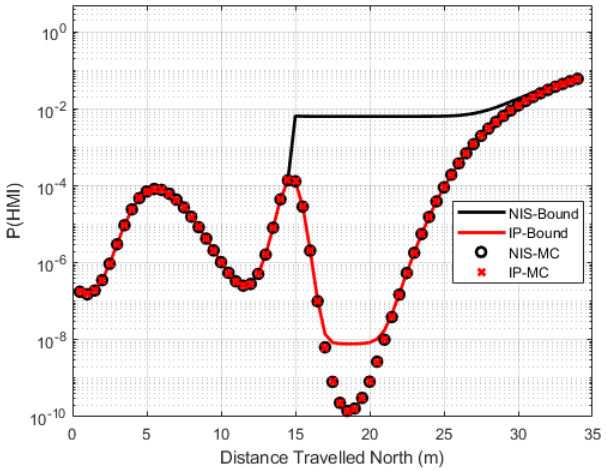

Fig. 6. Integrity Risk Bounds Using NIS Versus IP-Based Data Association for the Two-Landmark Scenario.

The covariance ellipses in Fig. 5 assume that CA is always achieved. In contrast, the integrity risk accounts for $P(CA)$. Fig. 6 shows $P(HMI_k)$ curves evaluated by direct simulation of random state prediction and measurement errors over 10,000 Monte Carlo (MC) trials. The actual risk curve for the IP method (red cross markers) matches that of the NIS approach (black circles). In parallel, $P(HMI_k)$-bounds are derived using (6) and (4) for NIS, and using (6) and (20) for IP, and are respectively shown in black and red. The two curves overlap for rover travel distances smaller than 15 meters and larger than 30 meters because over these two ranges, the $P(HMI_k \mid CA_K)$ term dominates in (6). For IP, the $P(HMI_k)$-bound approaches the actual risk over most of the trajectory. For travel distances 15-to-30 meters, the conservative $P(CA)$ bound dominates the NIS bound, but this is not the case for the IP approach that achieves orders of magnitude lower $P(HMI_k)$-bound values.

V. TESTING AND PERFORMANCE EVALUATION

In this section, we test the new DA IP-based method using actual data in a landmark-based navigation application using LiDAR/IMU. The LiDAR/IMU estimation methods was derived in [36].

Fig. 9 shows the experimental testbed that we designed to quantify $P(HMI_k)$ [36]. The testbed comprises a sensor-equipped rover moving on a figure-eight track, and an infrared (IR) camera motion capture system providing truth reference trajectory. The rover can operate for hours unattended to collect LiDAR and IMU data over repeated trajectory passes. We use a Velodyne's VLP-16 Puck LTE LiDAR and a NovAtel's IMU-IGM-A1 coupled with NovAtel's ProPak6. The IMU is set to record at 100 Hz sampling rate. The motion capture system includes twelve cameras, four VICON MX-T20s and eight Vantage 5s, which record the locations of small retro-reflective markers placed on the sensors and landmarks,

thus providing sub-centimeter level positioning and mapping at up to 200 Hz update rates. Data from all three sensors, IR cameras, LiDAR, and IMU, are time-tagged on a common computer clock and post-processed.

The landmarks used for navigation are four cylindrical landmarks. This simplistic test setup facilitates feature extraction and was chosen to avoid obscuring the analysis with extraction errors. In this case, the features are the coordinates in navigation frame of the intersection between a cylinder' axis and an arbitrary horizontal plane (e.g., the ground plane). In this implementation, we use a preset map of the cylinders. Our current feature extraction routine was evaluated in [36]. The test setup parameter values are listed in Table II.

We evaluate the localization performance of an IMU-aided LiDAR localization system. The IMU helps maintain an accurate measurement prediction $\mathbf{h}(\bar{\mathbf{x}})$.

In Fig. 10, the true and estimated trajectories are respectively represented with a thin black line and a thick blue line. They are overlapping. Rover positioning uncertainty is represented with red covariance ellipses. An inflation factor of 5 is used to facilitate visualization. Background shades of gray are used consistently across figures to identify segments of the rover trajectory: the dark gray area designates straight segments while light-gray and white areas respectively designate the top and bottom loops of the trajectory.

Fig. 11 displays $P(HMI_k)$-bounds using the NIS-based DA criterion in black, and using IP in red. The $P(HMI_k)$ bound is our safest estimate of the risk that the cross-track positioning error exceeds a 0.25 m alert limit. The NIS curve suggests that the term capturing the risk of WA quickly becomes prevalent in the NIS $P(HMI_k)$-bound, which thus increases monotonically and reaches 10^{-1} within the first 3 seconds. The bound stays at that level because $P(CA)$ in (8) is computed as a product of contributions over time: this risk contribution can only increase. In contrast, the IP-based bound remains lower than 10^{-5}. The red curve's variations reflect changes in positioning variance due to changes in the vehicle-to-landmark geometry as the rover moves.

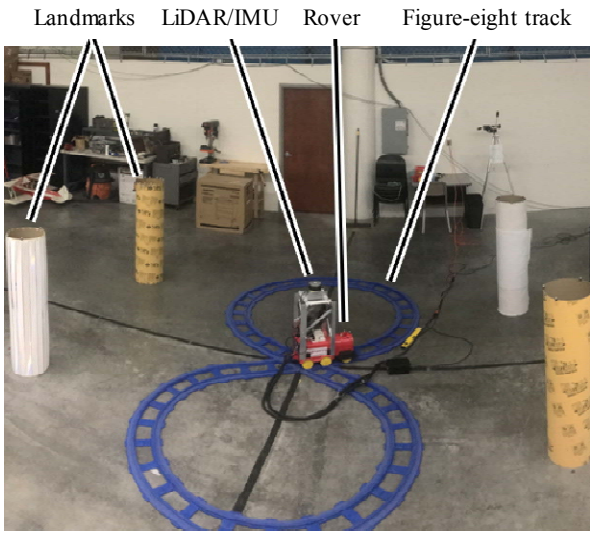

Fig. 7. Testbed Setup (VICON cameras at the ceiling are not shown)

TABLE II. TEST SETTINGS AND PARAMETERS

System Parameters	Values
Standard deviation of feature extraction ranging measurement	0.15 m
Standard deviation of feature extraction angular measurement	3 deg
Laser data sampling interval	0.1 s
Accelerometer velocity random walk	4.739 $m/s^2/\sqrt{Hz}$
Gyroscope angle random walk	17.244 $deg/\sqrt{hr}$
Accelerometer bias GMRP correlation time constant	3600 s
Gyroscope bias GMRP correlation time constant	3600 s
standard deviation of accelerometer GMRP bias	0.67 m/s^2
The standard deviation of Gyroscope GMRP bias	10 deg
IMU sampling time	0.01 s
Vehicle speed	0.6 m/s
Alert limit ℓ	0.25

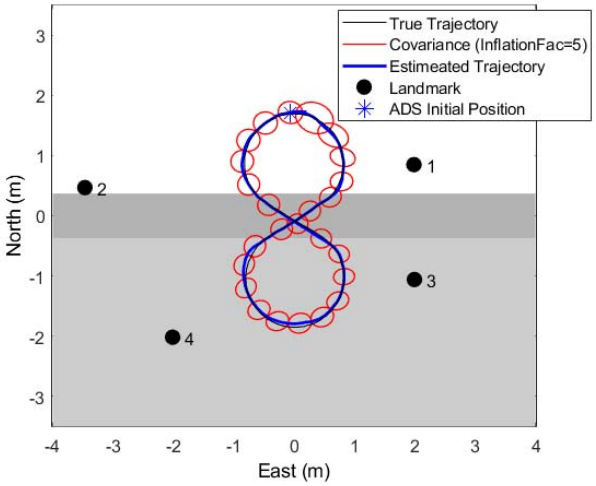

Fig. 8. Estimated Trajectory and Covariance Ellipses Using LiDAR/IMU

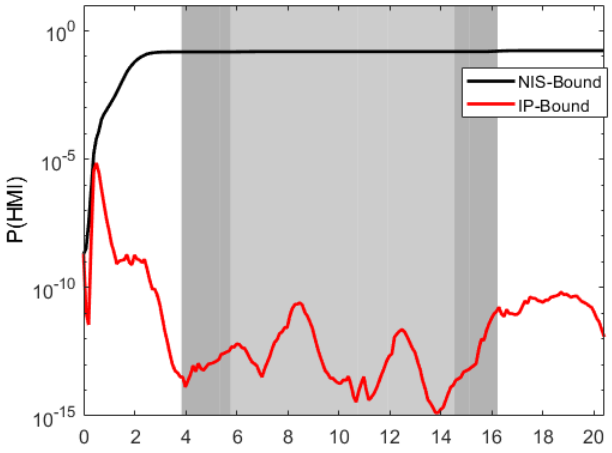

Fig. 9. Integrity Risk Bounds for the NIS Versus IP Data Association Criteria Using LiDAR/IMU

VI. Conclusion

In this paper, we develop a new approach to data association for multi-target tracking in autonomous vehicle landmark-based navigation using LiDAR/IMU. The new method determines correspondences between currently and previously observed targets using innovation projections (IP), as opposed to the more conventional criterion based on normalized innovation squared (NIS). The IP-based method provides a significant improvement in our ability to evaluate the risk of wrong associations (WA). We evaluated the new method using simulation and testing. The IP-based method demonstrated integrity risk levels orders of magnitude lower than the NIS method. Whereas the NIS risk bound inevitably increased as potential exposures to WA accumulated, the IP method stayed low.

References

[1] Y. Bar-Shalom, T. E. Fortmann, "Tracking and Data Association." *Mathematics in Science and Engineering*, Vol. 179, Academic Press, 1988.

[2] M. Joerger, and B. Pervan, "Measurement-Level Integration of Carrier-Phase GPS and Laser-Scanner for Outdoor Ground Vehicle Navigation," *ASME Journal of Dynamic Systems, Measurement, and Control*, Vol. 131, 2009.

[3] S. Thrun, "Robotic Mapping: A Survey," *Exploring Artificial Intelligence in the New Millenium*, G. Lakemeyer and B. Nebel, February 2002.

[4] J. Leonard and Durrant-Whyte, H. "Directed Sonar Sensing for Mobile Robot Navigation," *Kluwer Academic Publishers*, Cambridge, MA, pp. 129-138, 1992.

[5] S.B. Williams, Dissanayake, G. and Durrant-Whyte, H. "An efficient Approach to the Simultaneous Localisation and Mapping Problem," *Proc. IEEE-ICRA*, 2002.

[6] F. Lu and Milios, E. "Globally Consistent Range Scan Alignment for Environment Mapping," *Autonomous Robots 4*, pp. 333-349, 1997.

[7] T. Röfer "Using Histogram Correlation to Create Consistent Laser Scan Maps," *Proc. IEEE IROS-2002*, Lausanne, Switzerland, pp. 625-630, 2002.

[8] A. Diosi and Kleeman, L. "Laser scan matching in polar coordinates with application to SLAM," *Proc. IEEE/RSJ IROS,* 2005.

[9] O. Bengtsson and Baerveldt, A.J. "Robot localization based on scan-matching-estimating the covariance matrix for the IDC algorithm," *Robotics and Autonomous Systems*, Vol. 44, pp. 29–40, 2003.

[10] Elfes, "Occupancy grids: A probabilistic framework for robot perception and navigation," *Journal of Robotics and Automation*, Vol. 3, pp. 249–265, 1987.

[11] J. Choi, S. Ulbrich, B. Lichte and M. Maurer, "Multi-Target Tracking using a 3D-Lidar sensor for autonomous vehicles," *16th International IEEE Conference on Intelligent Transportation Systems (ITSC 2013)*, The Hague, pp. 881-886, 2013.

[12] S. Sato, M. Hashimoto, M. Takita, K. Takagi and T. Ogawa, "Multilayer lidar-based pedestrian tracking in urban environments," *2010 IEEE Intelligent Vehicles Symposium*, San Diego, CA, pp. 849-854, 2010.

[13] B.N. Vo and W.K. Ma. "The gaussian mixture probability hypothesis density filter," *IEEE Transactions on Signal Processing*, Vol. 54, No. 11, pp. 4091-4104, November 2006.

[14] J. Mullane, B. Vo, M. D. Adams and B. Vo, "A Random-Finite-Set Approach to Bayesian SLAM," *IEEE Transactions on Robotics*, Vol. 27, No. 2, pp. 268-282, April 2011.

[15] R. Mahler, "Multi-target bayes filtering via first-order multi-target moments," *IEEE Transactions on AES*, Vol. 4, No. 39, pp. 1152-1178, October 2003.

[16] J. Mullane, B. N. Vo, M. Adams, and W. S. Wijesoma, "A random set formulation for Bayesian SLAM," *Proc. IEEE/RSJ Int. Conf. Intell. Robots Syst.*, pp. 1043–1049, Sep. 2008.

[17] I. Tena Ruiz, Y. Petillot, D.M. Lane, and C. Salson, "Feature Extraction and Data Association for AUV Concurrent Mapping and Localisation," *Proc. IEEE-ICRA*, 2001.

[18] C. Estrada,.J. Neira, and J. Tardos, "Hierarchical SLAM: real-time accurate mapping of large environments,". *IEEE Transactions on Robotics*, Vol. 21, No. 4, 2005, pp.588-596.

[19] T. Bailey, "Mobile Robot Localisation and Mapping in Extensive Outdoor Environments," PhD Dissertation, University of Sydney, 2002.

[20] B. Bićanić, M. Oršić, I. Marković, S. Šegvić, I. Petrović, "Pedestrian Tracking by Probabilistic Data Association and Correspondence Embeddings," *22nd International Conference on Information Fusion (FUSION)*, 2019.

[21] H.Caiab, Y. Yangab, S. Gehlyab, S. Wua, K. Zhanga, "Improved tracklet association for space objects using short-arc optical measurements," *Acta Astronautica*, Vol. 151, , pp 836-847, 2018.

[22] L. Pirovano, G. Principe, R. Armellin, "Data association and uncertainty pruning for tracks determined on short arcs," *Celestial Mechanics and Dynamical Astronomy*, Vol. 132, No. 1, 2020.

[23] C.T. Bellows, "Leveraging External Sensor Data for Enhanced Space Situational Awareness," PhD Dissertation, Air Force Institute of Technology, 2015.

[24] S.-S. Jan and Y.-C. Kao, "Radar Tracking with an Interacting Multiple Model and Probabilistic Data Association Filter for Civil Aviation Applications," *Sensors,* Vol. 13, pp. 6636-6650, 2013.

[25] M. Jamoom, M. Joerger, and B. Pervan, "UAS Sense and Avoid Integrity and Continuity for Multiple Intruders," *Proceedings of IEEE/ION PLANS 2016*, Savannah, GA, 2016.

[26] G. Lee, and M. Joerger, "Integrity and Continuity of GPS-based Collision Warning Systems Using Vehicle-to-Vehicle Communication," *Proceedings of IEEE/ION Position, Location, and Navigation Symposium (PLANS 2018)*, Monterey, CA, 2018.

[27] A. Hunde, and B. Ayalew, "Automated Multi-Target Tracking in Public Traffic in the Presence of Data Association Uncertainty," *Annual American Control Conference (ACC)*, , pp.300-306, 2018.

[28] S. Thrun, W. Burgard, and D. Fox, "A probabilistic approach to concurrent mapping and localization for mobile robots," *Mach. Learn. Auton. Robots*, Vol. 31, No. 5, pp. 1–25, 1998.

[29] D. Maksarov and H. Durrant-Whyte, "Mobile vehicle navigation in unknown environments: A multiple hypothesis approach," *IEEE Control Theory Appl.*, Vol. 142, No. 4, pp. 385–400, 1995.

[30] A.J. Cooper, "A Comparison of Data Association Techniques for Simultaneous Localization and Mapping," M.S. Thesis, Massachussetts Institute of Technology, 2005.

[31] Y. Bar-Shalom, F. Daum, and J. Huang, "The probabilistic data association filter," *IEEE Control Syst. Mag.*, Vol. 29, No. 6, pp. 82–100, Dec. 2009.

[32] F. C. Chan, M. Joerger, S. Khanafseh, and B. Pervan, "Bayesian fault-tolerant position estimator and integrity risk bound for GNSS navigation," *J. Navig. Royal Inst. Navig.*, Vol. 67, pp. 753–775, 2014.

[33] J. Areta, Y. Bar-Shalom, R. Rothrock, "Misassociation Probability in M2TA and T2TA," *Journal of Advances in Information Fusion*, Vol. 2, No. 2, 2007.

[34] M. Joerger, and B. Pervan, "Quantifying Safety of Laser-Based Navigation," *IEEE Transactions on Aerospace and Electronic Systems*, Vol. 55, No. 1, 2019.

[35] G. Duenas Arana, M. Joerger, M. Spenko, "Recursive Integrity Monitoring for Mobile Robot Localization Safety," *International Conference on Robotics and Automation (ICRA)*, Montréal, Canada, 2019.

[36] A. Hassani, N. Morris, M. Spenko, and M. Joerger, "Experimental Integrity Evaluation of Tightly-Integrated IMU/LiDAR Including Return-Light Intensity Data," *Proceedings of the 32nd International Technical Meeting of The Satellite Division of the Institute of Navigation (ION GNSS+ 2019)*, Miami, FL, 2019.

[37] A. Hassani, G. Duenas Arena, M. Spenko, and M. Joerger, "LiDAR Data Association Risk Reduction Using Tight Integration with INS," *Proceedings of the 31st International Technical Meeting of The Satellite Division of the Institute of Navigation (ION GNSS+ 2018)*, Miami, FL, 2018.

[38] M. Joerger, G. Duenas Arana, M. Spenko, B. Pervan, "Landmark Data Selection and Unmapped Obstacle Detection in Lidar-Based Navigation," *IEEE Trans. Aerosp. Electron. Syst.* Portland, Oregon, pp. 1886–1903, 2017.

[39] M. Joerger, G. Duenas Arana, M. Spenko, and B. Pervan, "A New Approach to Unwanted-Object Detection in GNSS/LiDAR-Based Navigation," *Sensors – Special Issue: GNSS and Fusion with Other Sensors*, 2018.

[40] G. Duenas Arana, M. Joerger, and M. Spenko, "Local Nearest Neighbor Integrity Risk Evaluation for Robot Navigation," *Proceedings of IEEE International Conference on Robotics and Automation (ICRA2018)*, Brisbane, Australia, 2018.

[41] Radio Technical Commission for Aeronautics (RTCA) Special Committee 159, "Minimum Operational Performance Standards for GPS Local Area Augmentation System Airborne Equipment," *Document RTCA/DO-253B*, 2007.

[42] Radio Technical Commission for Aeronautics (RTCA) Special Committee 159, "Minimum Operational Performance Standards for Global Positioning System Wide Area Augmentation System Airborne Equipment," *Document RTCA/DO-229D*, 2006.

[43] International Civil Aviation Organization (ICAO), "Annex 10," *Aeronautical Telecommunications*, Volume 1 (Radio Navigation Aids), Amendment 84, 2009.

[44] U.S. Department of Transportation (DOT) National Highway Traffic Safety Administration (NHTSA), "Automated Driving Systems 2.0: A Vision for Safety," 2017.

[45] DOT Federal Highway Administration (FHWA), "Vehicle Positioning Trade Study for ITS Applications", *FHWA-JPO-12–064*, 2012.

[46] T. G. R. Reid, S. E. Houts, R. Cammarata, G. Mills, S. Agarwal, A. Vora, G. Pandey, "Localization Requirements for Autonomous Vehicles," *SAE International Journal of Connected and Automated Vehicles*, 2019.